

Neuron, Volume 100

Supplemental Information

**Brain-wide Organization of Neuronal Activity
and Convergent Sensorimotor Transformations
in Larval Zebrafish**

Xiuye Chen, Yu Mu, Yu Hu, Aaron T. Kuan, Maxim Nikitchenko, Owen Randlett, Alex B. Chen, Jeffery P. Gavornik, Haim Sompolinsky, Florian Engert, and Misha B. Ahrens

Figure S1 (Chen, Mu, et al.).

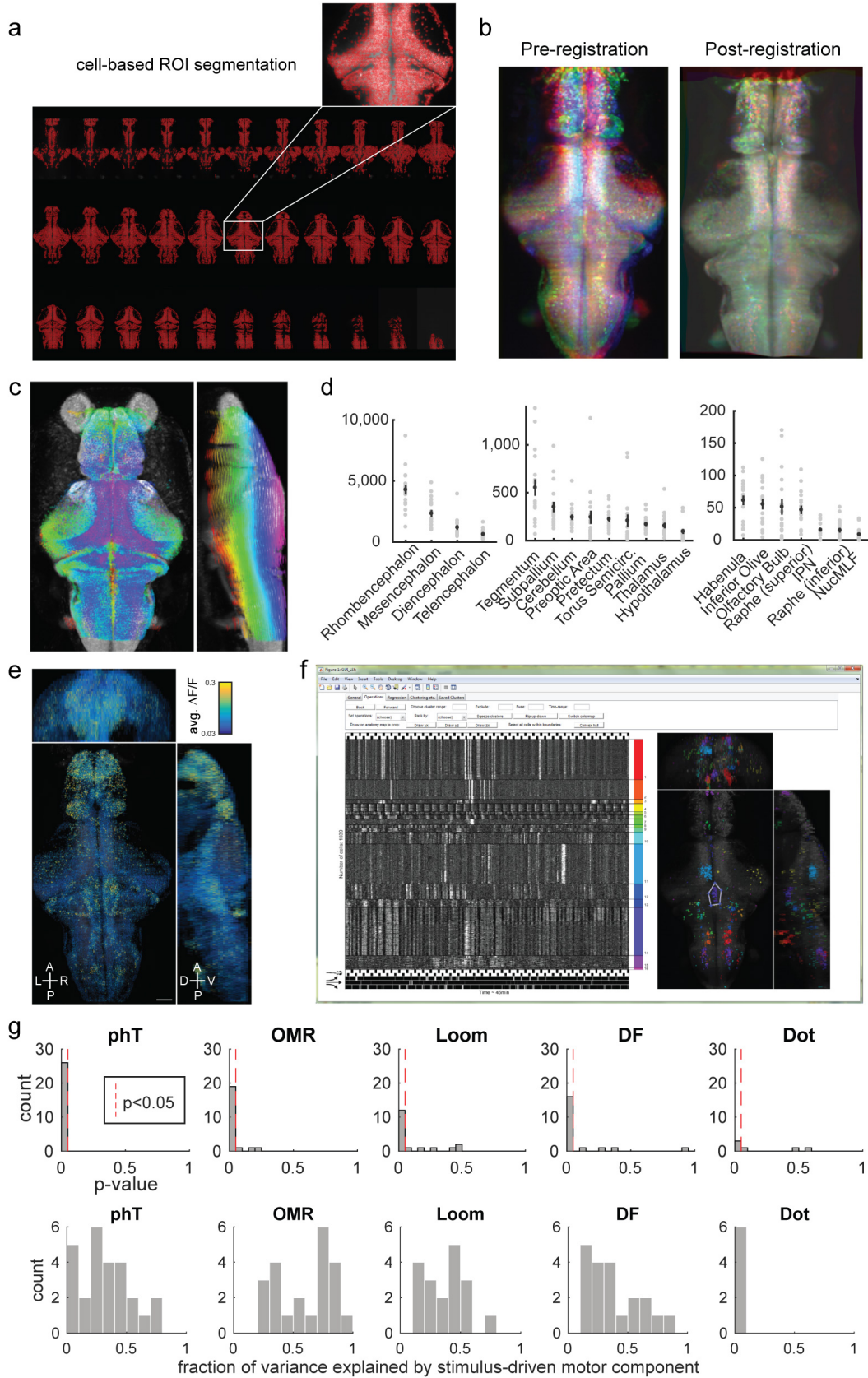


Figure S1. Related to Figure 1. (a) Results of automatic cell segmentation based on nucleus-localized calcium indicator. GCaMP6f was expressed panneuronally under the *e/av/3* promoter. Inset shows good coverage of segmented ROI's (red dots) within one imaging plane (total number of segmented ROI's in this animal: 92,538). (b) Overlaid z-projection image of three animals (shown in red/green/blue channels, respectively) before and after registration to an average image stack. (c) Registration to the Z-brain reference atlas. Pseudocolors are applied to the z-planes before registration (red through purple: ventral to dorsal). (d) Number of cells included in selected anatomical regions according to the Z-brain atlas. Left panel: main brain divisions. Middle and right panel: smaller regions and anatomical features. Grey dots represent data from individual animals (n=18), with mean±SEM shown in black. (e) Whole-brain calcium activity averaged per cell over time, shown in pseudo-colors, for one example animal. (f) Interface of the custom interactive software that was used to develop the analyses presented in this study. Snapshot shows selected neurons sorted into clusters (indicated by different colors), with their functional activity shown in grayscale in the left panel and their anatomical locations in the right panel. (g) Quantification of behavior for different stimulus paradigms. Upper row: p-values were calculated for comparing behavior during leftward stimulation to rightward stimulation (for dark flashes, dark-field versus bright-field was used instead). Behavioral readouts for the left side and the right side were calculated separately and pooled in histogram. For all stimuli except for moving dots ("dot"), the majority of datapoints are significant ($p < 0.05$). The dot stimulus was an attempt to to evoke prey-capture responses (Bianco et al., 2011; Trivedi and Bollmann, 2013). However, in our open-loop preparation, the moving dots stimuli did not reliably elicit directed swims, so we excluded the prey capture stimulus for ensuing analysis. Lower row: the fraction of variance explained by the stimulus-driven motor component, see Fig. 3 text and methods for stimulus-driven motor component. A value of 1 would be reached if the behavior is entire periodic (as is the stimulus). While it varies across fish (and left/right sides) how much the stimulus determines the behavior, the moving dots appears as a negative control here that does not elicit behavior.

Figure S2.

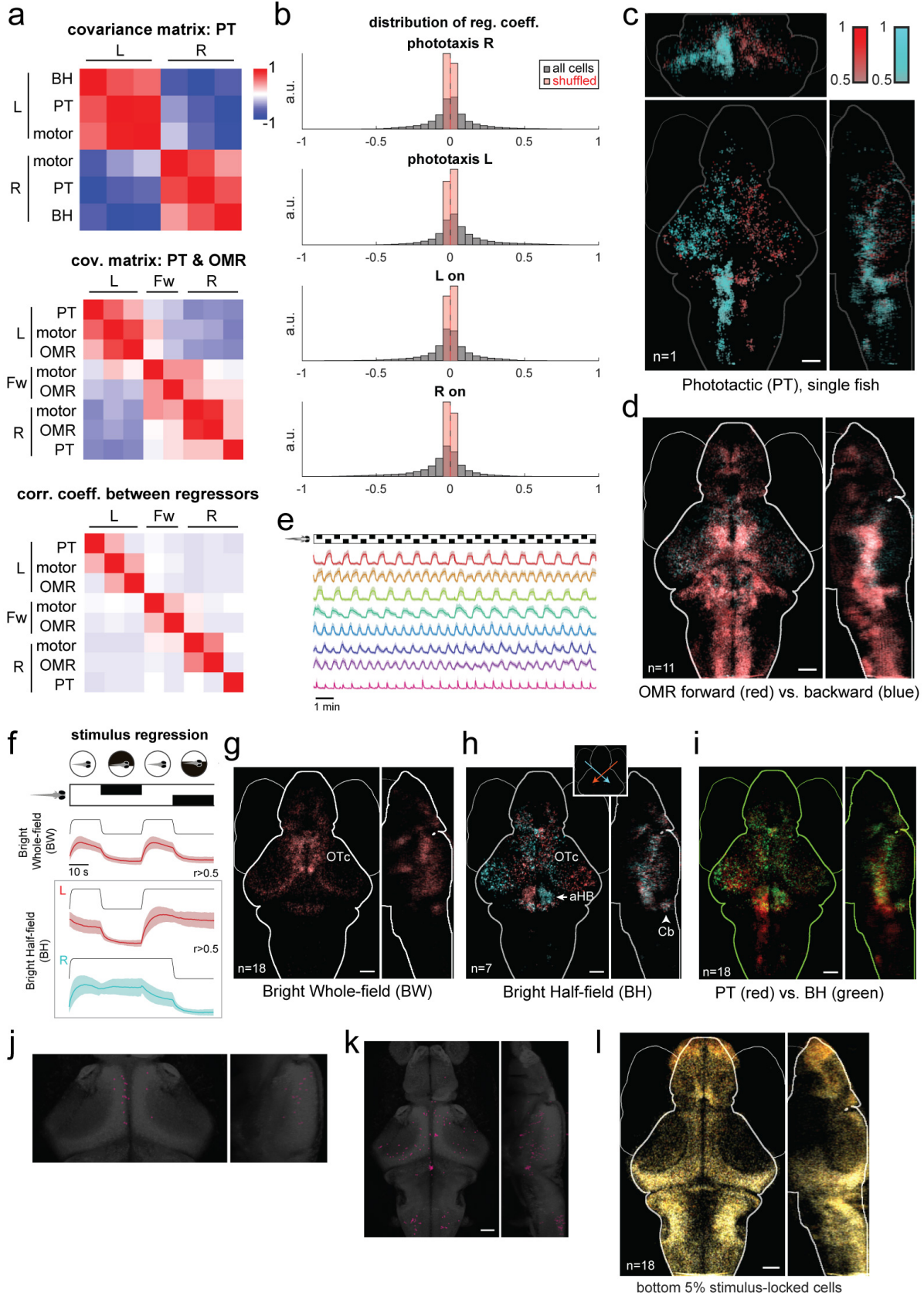


Figure S2. Related to Figure 2. (a) Correlation analyses between regressions, for single example fish. Top and middle panel: Covariance matrix or 'Representational Similarity matrix' (Kriegeskorte et al., 2008), showing the relationship between whole-brain responses characterized through the various stimulus/motor regressors (see Methods). phT: phototactic stimulus; BH: Bright half-field stimulus; see Fig. S2h. For the middle panel, moving stripes (OMR) were presented in left/right/forward/backward directions, and the fictive recording is parsed into left/right/forward swims regressors. Bottom panel: (direct) correlation coefficients between the regressors (without regressing over cells). This correlation analysis complements the visual comparison of tuning maps that only feature highly correlated neurons. (b) Histograms of regression coefficients for all cells from a representative fish, using various regressors. 'L(R) on': Bright half-field for the left (right) side being bright. Horizontal axis: Pearson correlation coefficient. (c) Single fish example of regression with phototactic regressors. Note that the left side of the hindbrain shows high levels of responses, indicating that leftwards swims are highly correlated with the leftward phototactic stimulus. The finer distinctions between stimulus responses and stimulus-driven motor responses are made in Figure 3. Such asymmetries in behavior (and the corresponding neural correlates) are also typical at the single-animal level (d) OMR regression map for forward and backward moving gratings. (e) Single-trial traces for the same clusters as in Fig. 2h. (f) Stimulus regressions using phototactic component regressors. Fish were shown a periodic stimulus during imaging that consists of leftwards and rightwards phototactic stimuli separated by a whole-field bright background. The stimulus regressors (black) are constructed by convolving a binary step function with an impulse kernel of GCaMP6. Bright whole-field and bright half-field regressors are shown. The colored traces show the average activity (mean \pm SD for all ROI's with $r>0.5$) for the same example fish as in Fig. 2a. (g) Map for bright whole-field regressor. (h) Map for the pair of bright half-field regressors. OTc: optic tectum. aHB: anterior hindbrain. Cb: cerebellum. (i) Comparison between phototactic stimulus regression (e, red channel) and bright half-field regression (d, green channel). (j) Map of cluster 8 from Fig. 2h. (k) Map of cluster 7 from Fig. 2i. (l) An average map of the least sensory-related cells (bottom 5% periodic, all stimulus types).

Figure S3.

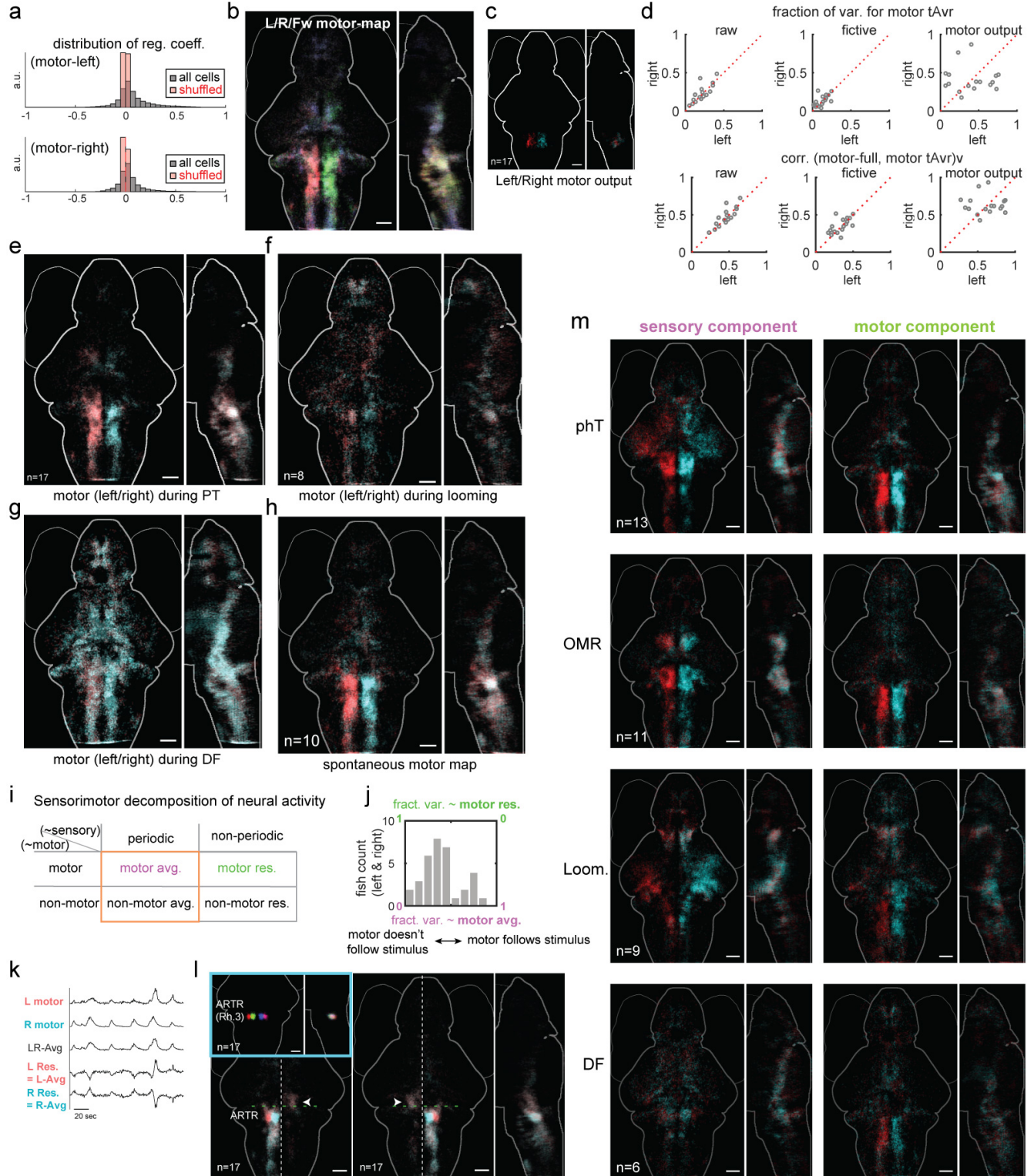


Figure S3. Related to Figure 3. (a) Histograms of motor regression coefficients for all cells from a representative fish, compared to shuffled traces in which cell activity was shuffled along the time axis. Many cells are correlated to the motor regressors above chance. Horizontal axis: Pearson correlation coefficient. (b) Three-way contrast map for left/right/forward swimming. Regression was performed using the 3 fictive swim regressors for left/right/forward (red/green/blue) respectively, and individual cells are colored based on their best regressor. (c) Average anatomical map of the cells used to define motor output (ROI's with highest correlation to the recorded fictive behavior, constrained within Rhombomeres 4 and 5; see Methods). Red: left motor; cyan: right motor. (d) Comparison between raw motor recordings, parsed fictive swims, and the motor output ('motor-seeds') extracted directed from calcium activity (see Methods). Upper row: fraction of variance explained by the trial-average (tAvr) component of the motor regressor. Lower row: correlation between the full motor regressor and the tAvr component of the motor regressor. The motor outputs showed increased variance explained and correlations, suggesting that they more faithfully represent motor activity patterns. (e-h) Motor regression map (similar to Fig. 3b) for (e) pH_T, (f) looming, (g) dark flash, and (h) spontaneous stimuli. (i) Schematic illustration of sensory-motor decomposition of neuronal activity into periodic/aperiodic and motor/non-motor components. (j) Histogram of the fraction of variance explained by the periodic component of the motor output (n=17 fish, left and right motor outputs calculated separately). (k) Illustration of the left/right motor average and residual. The residual for each side was calculated by subtracting the respective motor activity from the left/right average. (l) Regression maps using the average response of ARTR as regressor (Dunn et al., 2016). Inset: manually curated ROI's for ARTR, separating the medial and lateral stripe for each of the left/right side. Arrowhead: regression to the lateral ARTR stripes identifies cells in contralateral Rh.1. (m) Stimulus-driven (left) and independent (right) motor maps calculated from pH_T, OMR, Looming, and Dark Flash stimulus blocks. Analogous to Fig. 3e for OMR.

Figure S4.

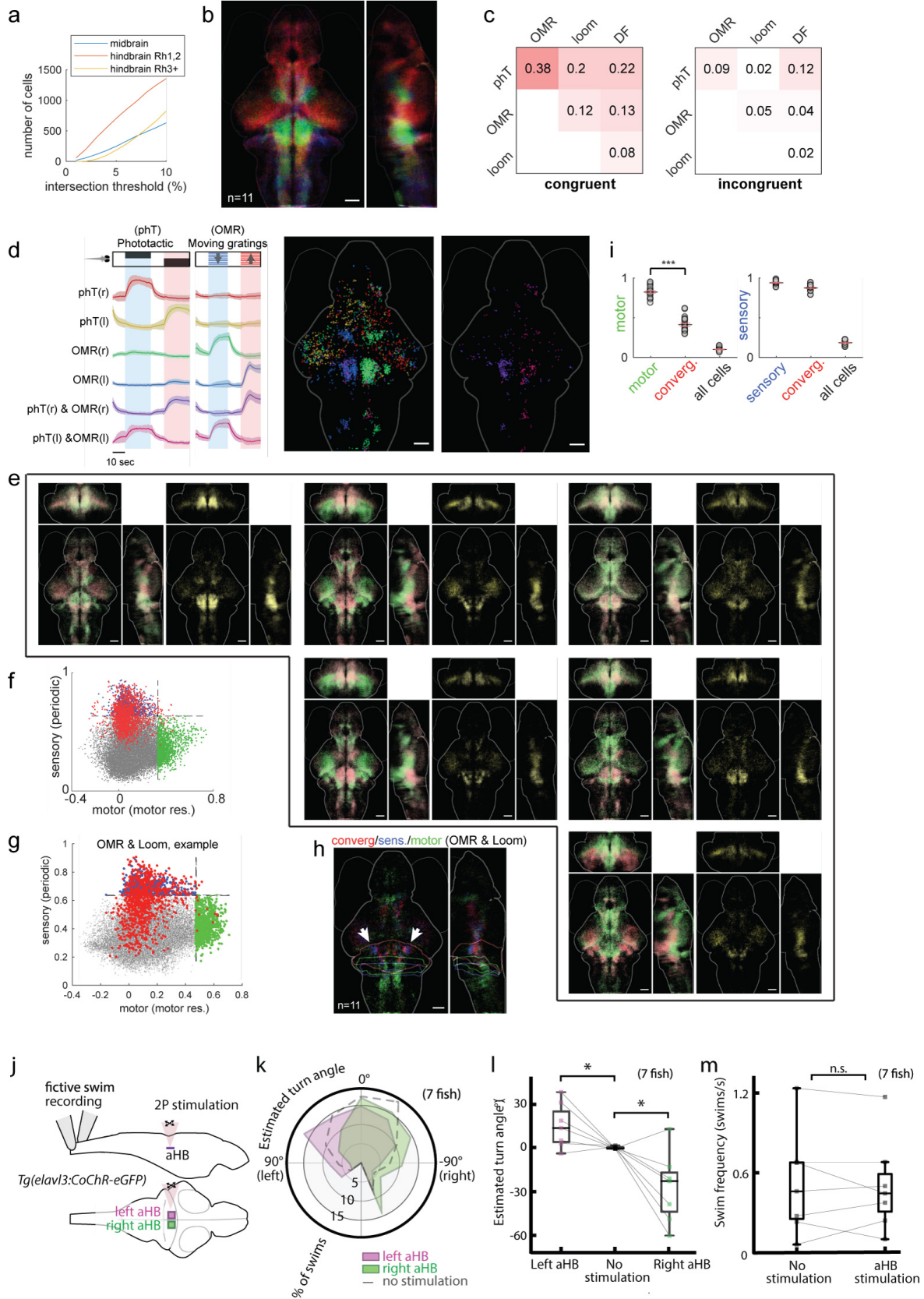


Figure S4. Related to Figure 4. (a) Number of convergent cells (for pH_T and OMR) as a function of threshold (rank %) for (1) midbrain (2) hindbrain Rh_{1,2} and (3) hindbrain Rh₃₊. Across the whole range of thresholds, the hindbrain Rh_{1,2} contains more than twice as many convergent cells than the midbrain and hindbrain Rh₃₊ regions. (b) RGB overlay image of pH_T only (red), OMR-only (blue) and joint-pH_T-OMR (green) cells. Individual cells selected by t-test $p < 0.001$ (leftward-stimulus selectivity contrasted with rightward-stimulus selectivity). (c) Quantification of the number of congruent (left) and incongruent (right) convergent cells for each stimulus pair. Number and shading indicate proportion of cells that are highly tuned (top 5%) to either stimulus. (d) Traces same as in Fig. 4b: whole-brain regressions were performed to a set of regressors that include pH_T specific-, OMR specific-, and pH_T&OMR joint-regressors. For cells that have a correlation coefficient > 0.4 to at least one of these regressors, they were classified by their best regressors into 6 groups, color-coded and identified by labels. Average functional activity of these 6 groups of neurons is shown (mean \pm SD). Corresponding anatomical maps shown at right. (Cells most highly tuned to motor outputs have been excluded here, by including motor regressors in this best-regressor analysis.) (e) Overlay of single-stimulus maps (left) and convergence maps (right) for each stimulus pair. The convergence maps are equivalent to Fig. 4c. (f) Same as Fig. 5e, except for right motor output (Fig. 5e shows data for left motor output). Note that convergent cell activity was less related to right motor output than left. Asymmetric left/right activity patterns and behavioral responses were not uncommon. (g) Example of plot analogous to Fig. 4g, except for OMR and Looming stimuli. All stimulus pairs have convergent cells (red) that have low motor residual components, indicating that they are sensory convergence cells. (h) Anatomical map of OMR/Looming convergence corresponding to Fig. S4g. (i) Related to Fig. 4g. Right: Regression coefficient to motor res. for (1) top 5% of cells by motor res. (2) top 5% convergent cells (3) all cells. Corresponds to the x values of the green, red, and gray dots in Fig. 5e, except for all fish and both left and right motor outputs. Note that convergent cells are significantly less motor-related than the most motor-related cells. Left: (Square root of) variance explained by their periodic component of activity for (1) top 5% of cells by periodicity (2) top 5% convergent cells (3) all cells. Corresponds to the y values of the blue, red, and gray dots in Fig. 4g, except for all fish and both left and right motor outputs. Note that convergent cells are as periodic as the most sensory-related cells. (j-m) Optogenetic stimulation of the anterior hindbrain biases turn direction but does not affect swim frequency. **j**: Schematic of setup for optogenetic stimulation and fictive behavior recording. **k**: Average distribution of swims elicited by forward grating with optogenetic stimulation of either the left anterior hindbrain (aHB) or right aHB, or forward grating without optogenetic stimulation. Left (90°) and right (-90°) were normalized to the mean turn angle elicited by left- or rightward grating, respectively. **l**: Optogenetic stimulation biases the mean turn angle in individual fish. (* : $p < 0.05$, Student's t-test). **m**: Optogenetic stimulation does not change swim frequency. Swim frequency was calculated as total number of swims divided by time.

Figure S5.

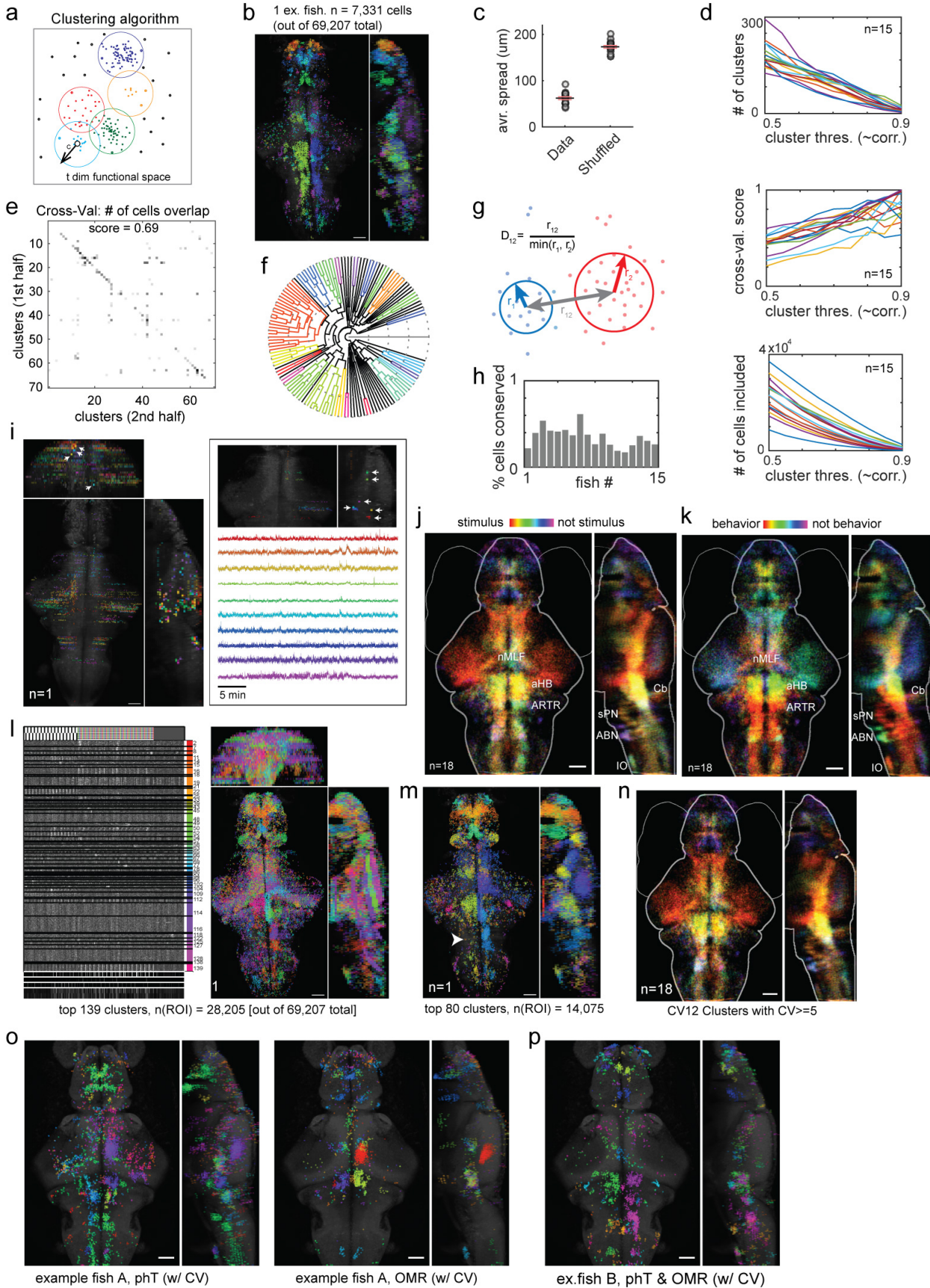


Figure S5. Related to Figure 5: clustering method. (a) Illustration of customized unsupervised clustering algorithm. A density based screen of all cells in functional space was followed by agglomerative clustering with an upper bound on within-cluster dissimilarity (see Methods). (b) Results of the automatic clustering algorithm applied to an example fish. The total 139 clusters (6,499 cells) were ordered by hierarchical clustering, and the rainbow colors were assigned based on the resulting leaf order. (c) Average distance within cluster per fish ($n = 18$ fish), for experimental data and a shuffled (simulated) control. Black line: population average; red lines: standard error. (d) Various clustering statistics as a function of clustering “stringency” threshold (which corresponds to a correlation value), for $n = 15$ fish (different colored lines). Top: number of clusters. Middle: two-fold cross validation scores, as in (e). Bottom: total number of cells included in all resulting clusters. A threshold of 0.7 was used to obtain results shown in Fig. 4. (e) Two-fold cross validation. Clusters produced from the first versus second half of the time-points of the data were matched, and a score was calculated as the fraction of number of cells that were assigned to matched clusters over the total number of cells. This was also visualized as the total “mass” distributed along the diagonal entries. (f) Hierarchical clustering diagram of clustering results for an example fish (not the same color code as (b)). (g) Illustration of the distance measure used in Fig 4I for assessing whether two clusters were conserved in anatomical space. (h) Per fish percentage of clusters (from automatic clustering results) that have anatomically corresponding clusters in at least 6 other fish (out of the 18 fish assessed) as in Fig 4I. (i) Clusters from the default clustering (stringency threshold = 0.7) that were identified as artifacts. Inset: for clarity, subset of clusters shown with functional traces. For most of these clusters, the cells within the cluster were aligned along one dimension, e.g. their projections appear as very dense dots (arrows). The dimension corresponds to one of the two laser scanning directions (anterior-posterior, and left-right). A simple script was used to screen out clusters that have very small standard deviation along these physical dimensions. (j-k) Left: average map of functional clusters colored by rank as stimulus-locked (i.e. periodic) (red) to not stimulus locked (purple). Right: average map of functional clusters colored by rank for motor res., from most motor related (higher regression coefficients) (red) to least motor related (purple). Similar to single fish map shown in Fig. 5c-d. (l-m) Spatial ICA (Hyvärinen and Oja, 2000) as comparison to our clustering method. (l) Functional activity and anatomical map of ICA clusters (number of clusters matching that of our clustering method for better comparison). (m) A smaller selection of clusters with higher within-cluster correlation shown for clarity. The left half of the hindbrain motor area (arrowhead) is missing. (n) Anatomical map of cross-validated clusters (colors ranked as in Fig. 4j), averaged across all fish. Clusters with at least 5 corresponding cells across cross-validation sets were selected. (o) Within stimulus cross-validated clusters for phototaxis (left) and OMR (right), single fish example. (p) Matched between phototaxis and OMR, single fish example. w/ CV: only clusters matched by cross-validation as in (e) are shown.

Figure S6.

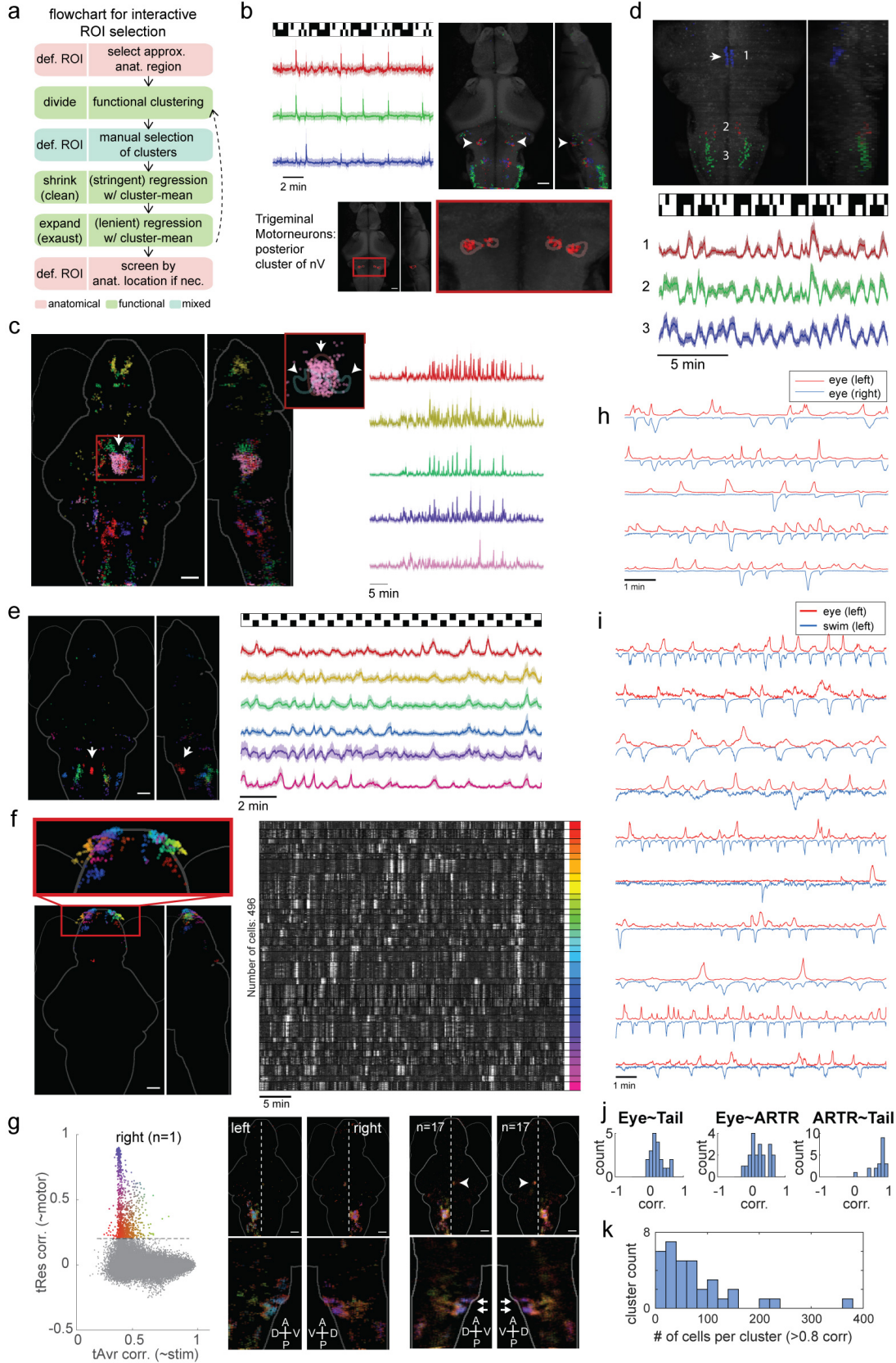


Figure S6. Related to Figure 5: selection of functional clusters. (a) Flowchart for interactive ROI selection (using the GUI), showing approximate guidelines. (b) Identification of a distinct network related to the trigeminal motor neurons (posterior clusters of nV, arrowheads) which are known for jaw movement control. The functionally identified cluster is characterized by strong, exceptionally sparse firing above a quiet baseline (shown in a representative fish). Red/green/blue: network divided into three clusters by k-means that show subtle differences; signal/noise was highest for the green cluster. Inset: anatomical masks for the trigeminal motor neurons from the Z-brain reference atlas - some of these neurons were located within the mask locations. (c) Mesencephalic locomotion-related region (pink cluster) and related functional network, shown as a total of 5 k-means clusters (distinct colors). Inset: pink cluster shown with anatomical masks from Z-Brain Atlas. Arrow: (red) mask for “Mesencephalon vglut2 cluster 1”. Arrowheads: pair of (green) masks for Mesencephalon nucMLF (nucleus of the medial longitudinal fascicle). Right: Average functional activity of clusters showing Mesencephalic locomotion-related networks. The activity of the cluster in pink is highly related to the forward swimming network, yet distinct from other clusters within the network. (d) Raphe networks. Left: dorsal raphe nucleus and related networks, shown as 3 k-means clusters. Arrow: dorsal raphe nucleus (as identified by functional clustering). (e) Inferior raphe nucleus and related network, shown as 6 k-means clusters. Regression to the raphe activity consistently revealed two symmetrical groups of neurons in the caudal hindbrain that coincide with the anatomical map of the vagus motor (nX) neurons that control gill movement, suggesting an intriguing functional connection between the two systems. (f) Olfactory bulb functional clusters. Left: map of 31 automatically identified clusters shown in different colors (colors assigned according to hierarchical ranking of clusters). Inset: Olfactory bulb region. Clusters corresponding to subnetwork outlined in red in the correlation matrix in Fig. 5i. Although their functional activity was not highly correlated between clusters, they shared a similar “texture” in the temporal domain. We hypothesize that these clusters represent the functional organization of the olfactory bulb, possibly demonstrating spontaneous activity, given a lack of (intentional) olfactory stimulation in our experiments. (g) Related to Fig. 5q,r. Left: Two-dimensional sensory-motor plot as in Fig. 5q, showing activity related to right motor output (Fig. 5q is left). Middle: Similar to Fig. 5r, but showing both right and left motor output maps (Fig 5r is the same as the lower left panel). Right: Same analysis as middle, but averaged for n=17 fish. (h) Left and right eye-movement traces, extracted from averaging the neural activity of highly concerted abducens nucleus functional clusters. (i) Comparison of eye-movement traces extracted from the abducens nucleus (ABD, in red) to the swimming motor output (blue). Each line is from a different fish, example data here shown for the OMR stimulus period. The ABD traces are mostly irregular while the motor traces follow the periodic stimulus. (j) For each side (left/right) of each fish, the correlation between the ABD eye trace, the motor output, and the HBO activity trace is compared in 3 histograms. This shows that the HBO activity is distinct from the ABD activity, while the HBO activity is highly correlated to the motor output. This finding is evidence against the contended hypothesis that the HBO is related to the bias in eye movement. (k) Histogram of number of cells within OCM clusters that were very highly correlated to the cluster mean (>0.8 correlation). Results shown for n = 17 fish, with 2 OCM clusters per fish.

Suppl. Movie 1. Single-trial (non-trial-averaged) whole-brain calcium activity in pan-neuronally expressed nucleus-localized GCaMP6f during presentation of phototactic stimuli, top (dorsal) maximum-intensity projection. Red dots: stimulus indicator (left/right). White dots: motor indicator for leftwards/rightwards swimming. Playback speed: 6.5x real speed. Related to Figure 1.

Suppl. Movie 2. Single-trial (non-trial-averaged) whole-brain calcium activity in pan-neuronally expressed nucleus-localized GCaMP6f during presentation of OMR stimuli, top (dorsal) maximum-intensity projection. Red dots: stimulus indicator (left/right/forward). White dots: motor indicator for leftwards/rightwards swimming. Playback speed: 6.5x real speed. Related to Figure 1.

Suppl. References

Bianco, I.H., Kampff, A.R., and Engert, F. (2011). Prey Capture Behavior Evoked by Simple Visual Stimuli in Larval Zebrafish. *Front. Syst. Neurosci.* 5, 1–13.

Dunn, T.W., Mu, Y., Narayan, S., Randlett, O., Naumann, E.A., Yang, C.-T., Schier, A.F., Freeman, J., Engert, F., and Ahrens, M.B. (2016). Brain-wide mapping of neural activity controlling zebrafish exploratory locomotion. *Elife* 5.

Hyvärinen, A., and Oja, E. (2000). Independent component analysis: Algorithms and applications. *Neural Networks* 13, 411–430.

Kriegeskorte, N., Mur, M., Ruff, D. a., Kiani, R., Bodurka, J., Esteky, H., Tanaka, K., and Bandettini, P. a. (2008). Matching Categorical Object Representations in Inferior Temporal Cortex of Man and Monkey. *Neuron* 60, 1126–1141.

Trivedi, C.A., and Bollmann, J.H. (2013). Visually driven chaining of elementary swim patterns into a goal-directed motor sequence: a virtual reality study of zebrafish prey capture. *Front. Neural Circuits* 7, 1–18.